



Cascade charge separation mechanism by ternary heterostructured BiPO₄/TiO₂/g-C₃N₄ photocatalyst

Sergio Obregón^a, Yunfan Zhang^b, Gerardo Colón^{a,*}

^a Instituto de Ciencia de Materiales, Centro Mixto Universidad de Sevilla-CSIC, Américo Vespucio, 49, 41092 Sevilla, Spain

^b Laboratory of Green Chemistry, Faculty of Technology, Lappeenranta University of Technology, Mikkeli FI-50100, Finland

ARTICLE INFO

Article history:

Received 27 July 2015

Received in revised form

17 November 2015

Accepted 18 November 2015

Available online 22 November 2015

Keywords:

TiO₂

gC₃N₄

BiPO₄

Heterojunction

Photocatalytic activity

Phenol

ABSTRACT

A complex ternary BiPO₄/TiO₂/g-C₃N₄ heterostructure has been obtained from a simple impregnation method having good photoactivities for the degradation of phenol under solar-like irradiation. From the wide structural, surface and electronic characterization, we have stated that the formation of the ternary heterojunction notably affect photoactivity of pristine TiO₂. Thus, the best result for the binary system was obtained for 70 wt% TiO₂-30 wt% BiPO₄ system. The incorporation of g-C₃N₄ leads to a further improvement on the photocatalytic activity when it is specifically done over TiO₂. By means of photoluminescence spectroscopy and reactive oxygen species formation test, we propose that the effective charge carrier separation is taking place through a cascade-driven electronic mechanism. Therefore, by choosing the adequate band-engineering tailoring an important improved photoactivity can be achieved.

© 2015 Elsevier B.V. All rights reserved.

1. Introduction

The photocatalytic degradation of organic pollutants is becoming one of the most promising green chemistry technology [1,2]. The improvement and optimization of TiO₂ as photocatalyst is an important task for technical applications of heterogeneous photocatalysis in the future. In this sense, many investigations on the basic principles and enhancement of the photocatalytic activity either in the ultraviolet or visible region have been carried out [3,4]. Within the general scheme of a photoinduced processes, in order to translate the photon absorptivity in a semiconducting photocatalyst into surface photoactivity, generated charge carriers must reach the surface with high probability and be stabilized at the surface for electron/hole transfer processes (and not for recombination events). Therefore many attempts were made for the improvement of the photocatalytic efficiency by inducing the separation of photogenerated charges. In the past decades, numerous methods have been developed to increase the photocatalytic efficiency of TiO₂, such as cationic doping (Cr, Fe, V) [5–7], and anionic doping (N, C, B, S) [8–10] of TiO₂ in order to increase the visible light absorbance. Moreover, it is widely accepted that the final photoac-

tivity is strongly affected by the effective migration of generated charge carriers to the surface and its further transfer processes. Therefore a great effort was made in the last years for the improvement of the photocatalytic efficiency by inducing the separation of photogenerated charges. Among these approaches some authors invoked the use of noble metal co-catalysts such as Pt, Rh or Au [11,12]. On the other hand, carbon-like materials such as carbon nanotubes, graphene or carbon nitride have also served for this purpose [13–15]. A second approach widely reported passed through the coupling of TiO₂ with other semiconductors to increase the separation efficiency of photogenerated electron-hole pairs during photocatalysis mechanism [16–19]. This way, two important effects can be accomplished. On one hand, the increase of the separation efficiency of photogenerated electron-hole pairs during photocatalysis mechanism [20,21]; secondly, the extension of the absorption range of the photoactive system [22,23]. On this basis, it has been stated that recent advances in the tailoring of new photocatalysts for solar applications might defectively afford the comprehension of the band electronic structure and the effective handling of the photogenerated charge carriers [24].

In the present paper, we report the preparation of a complex ternary BiPO₄/TiO₂/g-C₃N₄ composite which clearly denotes an interesting synergistic improvement. Such better photocatalytic performance has been achieved by tailoring the synthetic proce-

* Corresponding author.

E-mail address: gcolon@icmse.csic.es (G. Colón).

dure and by taking into account the relative conduction and valence band positions of the single semiconductors.

2. Experimental

2.1. Sample preparation

2.1.1. Synthesis of single systems

The synthesis of BiPO₄ has been carried out by following a two-steps solvothermal procedure described elsewhere [25]. Briefly, 3 mmol Bi(NO₃)₃·5H₂O was firstly dissolved into a beaker with 100 mL of ethylene glycol (EG) under magnetic stirred at room temperature. Then, an equal amount of sodium phosphate (Na₃PO₄·12H₂O) were added to the bismuth nitrate solution under vigorous stirring for 15 h. As a result a white suspension was gradually formed during the entire stirring process. The precursor was obtained by separating the white suspension from EG by high speed centrifugation (11000 rpm, 10 min) and subsequently washed with ethanol three times. In the second step, the as-obtained precursor and 30 mL of H₃PO₄ solution (12 M) were transferred into a Teflon-lined stainless steel autoclave and heated at 160 °C for 6 h. Then the final product was attained via filtering, washing with ethanol three times, and subsequently drying at 60 °C for 24 h.

TiO₂ sample was obtained by means of a hydrothermal method elsewhere described [26]. Firstly, a TiO₂ colloidal solution was obtained by adding certain amount of Ti⁴⁺-isopropanol solution to 400 mL of distilled water at pH 2 achieved by means of acetic acid. After titanium isopropoxide (TTiP) addition a white precipitate is obtained. Then, upon stirring at room temperature for one week this suspension evolves to a milky homogeneous solution. A certain amount of triethylamine (TEA) was then added drop wise to the Ti-solution aliquot till the pH value was 9. Afterwards, the obtained white precipitate suspension was then placed in a Teflon recipient inside of stainless steel autoclave reactor. The hydrothermal treatment was performed at 120 °C, 20 h. The as obtained precipitate was then filtered, repeatedly washed and dried overnight at 120 °C. Then TiO₂ powder was submitted to a further calcination treatment at 300 °C for 2 h.

Finally, gC₃N₄ was obtained by simple calcination of melamine (Aldrich) at 580 °C (5 °C/min heating rate) for 4 h in a covered alumina crucible in order to prevent sublimation of melamine [27]. Evidence of the formation of gC₃N₄ can be found in a previous paper [28].

2.1.2. Synthesis of composite systems

TiO₂-BiPO₄ composites (hereafter TBP) with different wt% of BiPO₄ (ranged between 0 and 60 wt%) were prepared by a simple impregnation method [29]. Thus, the adequate amounts of TiO₂ and BiPO₄ were added into methanol and sonicated separately for 30 min. Then these two solutions were mixed and stirred at room temperature for 24 h. Afterwards, the composite photocatalysts

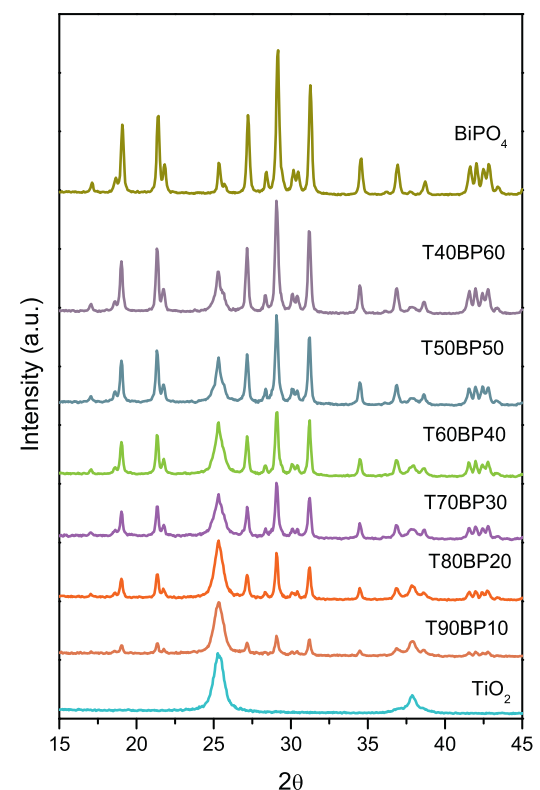
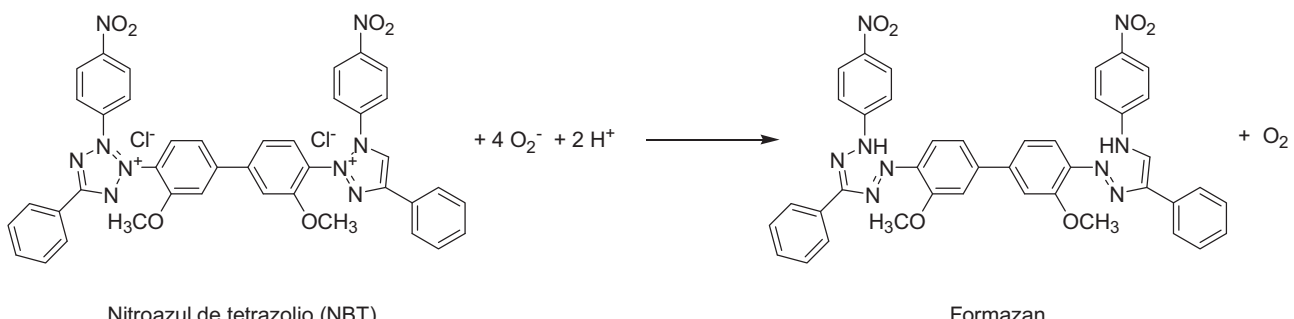


Fig. 1. XRD patterns for TiO₂-BiPO₄ heterostructures.

were obtained by evaporating the methanol under rotary evaporator at 80 °C. Hereafter, this set of samples will be named as TxPy, being x and y the wt% of each semiconductor.

For the preparation of the ternary heterostructure we will assemble BiPO₄ and TiO₂-gC₃N₄. Thus, carbon nitride-TiO₂ composites were achieved by the impregnation method above described. In a typical procedure, the appropriate gC₃N₄ (2 wt% with respect to TiO₂) and TiO₂ methanol suspensions were separately sonicated for 30 min. Then these two solutions were mixed and stirred at room temperature for 24 h. Afterwards, the composite photocatalysts were obtained by evaporating the methanol under rotary evaporator at 80 °C.

Finally, the ternary heterostructured TiO₂-gC₃N₄-BiPO₄ system was achieved by the same impregnation above described, using TiO₂-gC₃N₄ and BiPO₄. This way, we selectively deposit the BiPO₄ particles over the firstly formed TiO₂-gC₃N₄ heterojunction. These systems will be labelled as TCNxPy, being x and y the wt% of TiO₂-gC₃N₄ and BiPO₄ respectively.



Scheme 1. Reaction pathway between NBT and superoxide radicals with the formation of formazan.

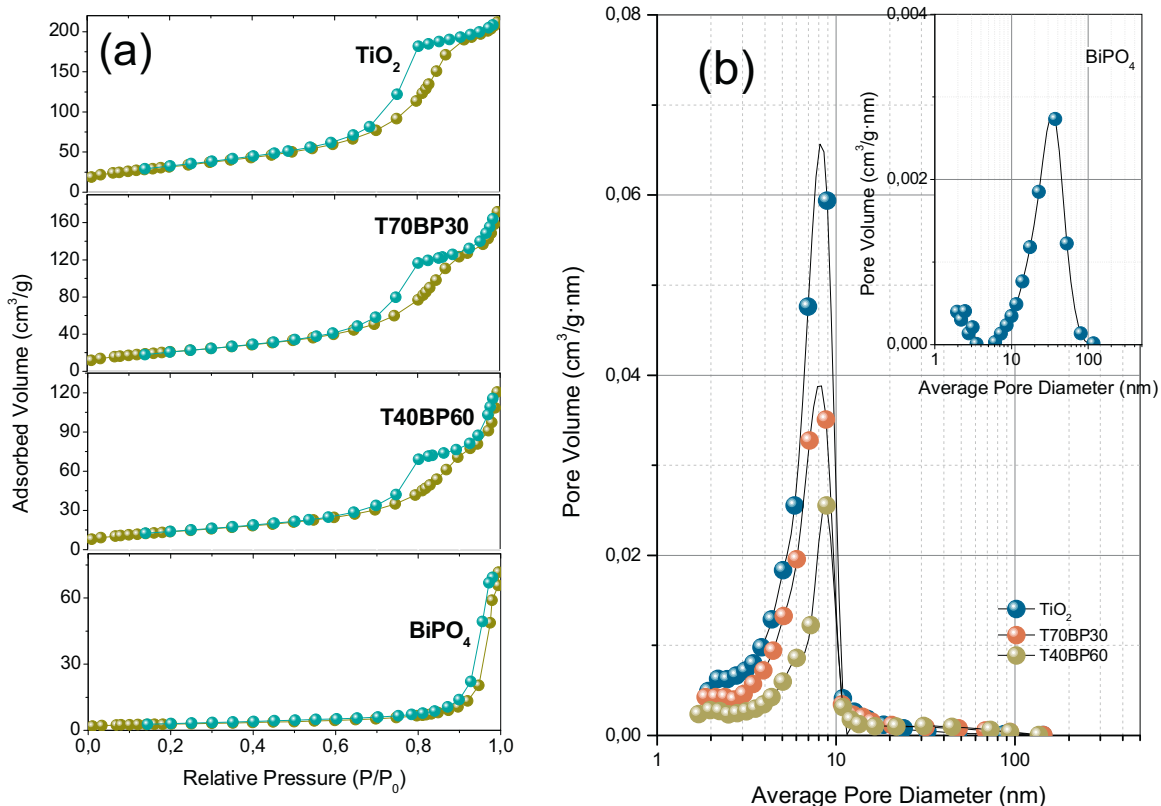


Fig. 2. (a) N_2 adsorption–desorption isotherms; (b) pore size distribution plots for TiO_2 -BiPO₄ heterostructures.

Table 1

Surface area, band gap values and photocatalytic activity for TiO_2 -BiPO₄ heterostructured systems.

Samples	BET (m^2/g)	Band gap (eV)	Reaction rate ($10^{-8} \text{ mol L}^{-1} \text{ s}^{-1}$)
BiPO ₄	9	4.10 _{BP}	0.00
T40BP60	50	3.17 _T	4.67
T50BP50	63	3.18 _T	5.43
T60BP40	70	3.17 _T	6.19
70BP30	77	3.19 _T	6.59
T80BP20	90	3.17 _T	5.96
T90BP10	105	3.17 _T	5.23
TiO_2	115	3.18 _T	4.93
TCN50BP50	60	—	6.40
TCN60BP40	74	—	6.92
TCN70BP30	86	—	7.26

Note: BP: BiPO₄; T: TiO_2 ; CN: gC₃N₄.

2.2. Characterization

The X-ray diffraction patterns of the synthesized product were measured by a Siemens D-501 diffractometer with Ni filter and graphite monochromator. The Cu K α radiation with wavelength of 0.15406 nm was used as X-ray source and all the patterns were recorded from $2\theta = 10\text{--}80^\circ$ with a scanning step of 0.05°.

The morphology of samples was characterized by means of transmission electron microscope (TEM) (Philips CM-200). The samples were dispersed in ethanol using an ultrasonicator and dropped on a carbon grid.

The UV-vis diffuse reflectance spectrum (Shimadzu, UV2101) were recorded in the wavelength range between 220 and 800 nm. The BaSO₄ was used as a reference.

BET surface area and porosity measurements were carried out by N_2 adsorption at -196°C using a Micromeritics ASAP 2010 instrument.

In order to investigate the recombination of photogenerated electrons/holes in the photocatalysts, the photoluminescence (PL) emission spectra of the samples were recorded. Room temperature PL emission spectra of the catalysts were recorded in a Horiba Jobin-Yvon Fluorolog3 spectrofluorometer operating in the front face mode.

The amount of O₂[−] generated during the photocatalytic reaction was monitored through the evolution of NBT (nitroblue tetrazolium), having an absorption maximum at 259 nm. NBT can be specifically reduced by photogenerated O₂[−] forming the insoluble purple formazan forms in the aqueous solutions (Scheme 1) [30]. Thus, the photocatalyst (1 g/L) and the NBT (2.5×10^{-5} mol/L) suspensions were ultrasonic treated for 15 min in the dark before the reactions. Then, these suspensions were irradiated by using an arc lamp source (Oriel Instruments) equipped with an Hg-Xe lamp of 200 W. The reactions were stopped by removing the catalyst particles from the suspensions through centrifugation (microcentrifuge Minispin, Eppendorf). The production of O₂[−] was quantitatively analysed by detecting the decrease of the concentration of NBT in the supernatant solutions with UV-vis spectrophotometer (Shimadzu, UV2101).

2.3. Evaluation of photocatalytic performance

Phenol oxidation reactions were performed using a batch reactor (250 mL) using an arc lamp source (Oriel Instruments) equipped with an Hg-Xe lamp of 200 W. In the oxidation tests, an oxygen flow was employed what produces a homogenous suspension of the catalyst in the solution. Before each experiment, the catalysts (1 g/L) were settled in suspension with the reagent mixture for 15 min. The evolution of the initial phenol concentration (ca. 20 ppm) was followed through the evolution of the characteristic 270 nm band

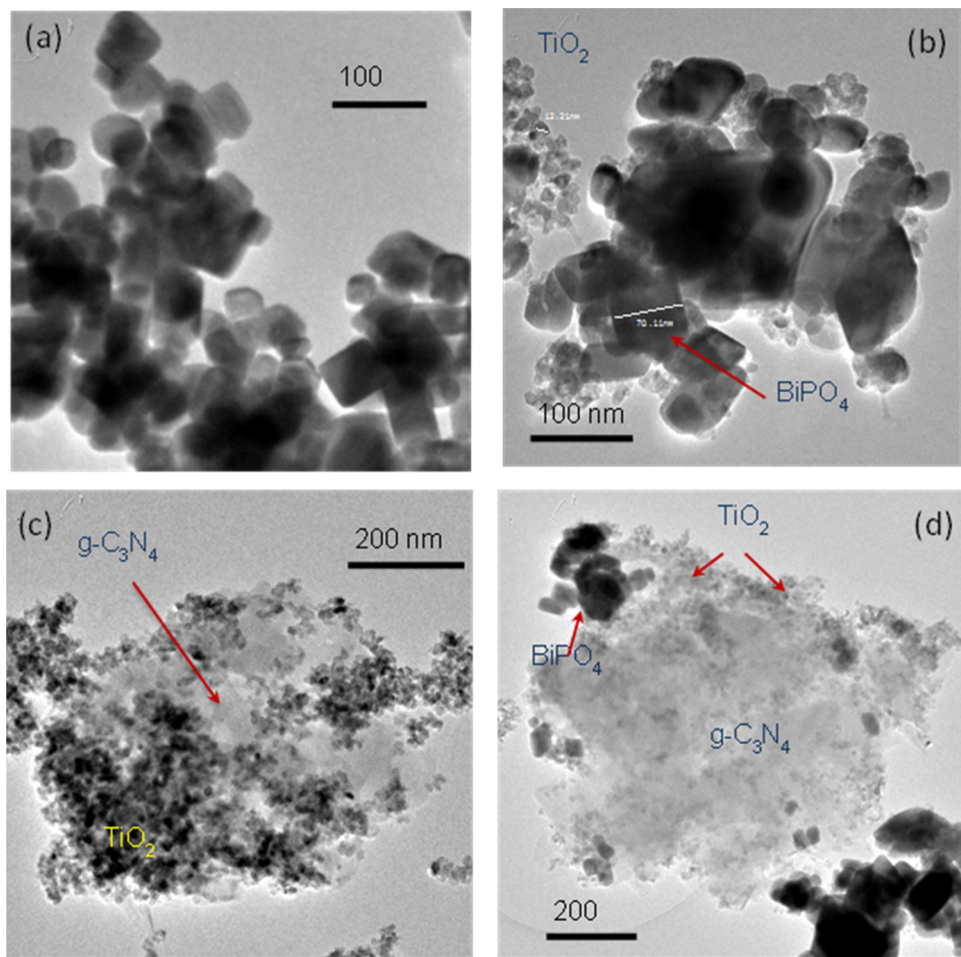


Fig. 3. Selected TEM images for (a) BiPO₄; (b) TiO₂-BiPO₄ (T70BP30); (c) TiO₂-gC₃N₄; (d) gC₃N₄-TiO₂-BiPO₄ (TCN70BP30) heterostructures.

using a centrifuged aliquot ca. 2 mL of the suspension (microcentrifuge Minispin, Eppendorf).

3. Results and discussion

The obtained pristine TiO₂ and BiPO₄ systems show well-crystallized diffraction patterns corresponding to anatase (PDF 21-1272) and low temperature monoclinic phase (PDF 15-0767) respectively (Fig. 1). From peak broadening (FWHM) and using the Scherrer equation, the crystallite size for TiO₂ and BiPO₄ result in 12 nm and 80 nm respectively. The composite TiO₂-BiPO₄ systems show both crystalline structures. It can be notice a clear evolution of low temperature monoclinic phase (LTMP) as BiPO₄ content increases, indicating the properly assembly of both semiconductors.

In Fig. 2, we depict the N₂ adsorption-desorption isotherms for single semiconductors and selected TBP systems. As it can be noticed, TiO₂ and BiPO₄ show highly different surface features. In both cases a type IV isotherm with clear H1 type adsorption hysteresis loop has been obtained, denoting the narrow distribution mesoporous character of the systems. The TBP composites show an isotherm resulting from the mixture of pristine material ones. Moreover, the obtained specific surface area for those systems appears clearly different (Table 1). As BiPO₄ is incorporated, the specific surface area progressively decreases. By observing the pore size distribution (Fig. 2b), it is evident the different average pore size for single systems. Thus, while in the case of TiO₂ a narrow mean pore size of 8 nm is found, for BiPO₄ the average size is

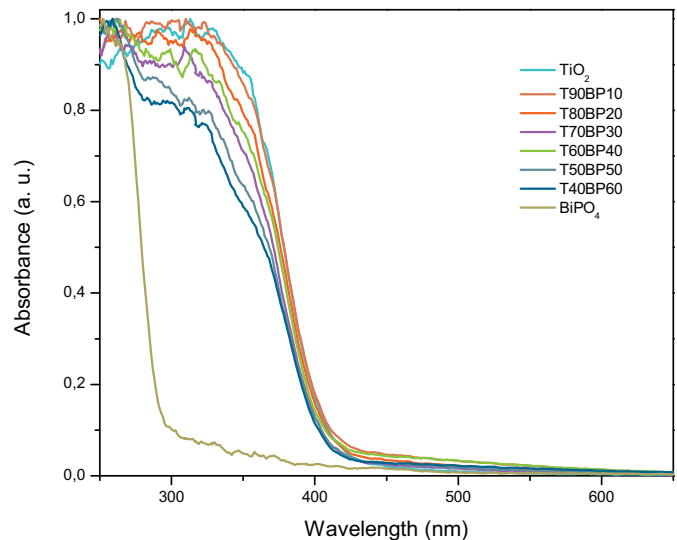


Fig. 4. Diffuse reflectance UV-vis spectra for TiO₂-BiPO₄ heterostructures.

located around 35 nm. As it can be stated from the hysteresis loop in the adsorption-desorption isotherm, the existing pore family in TiO₂ and BiPO₄ shows no connectivity.

The morphology of the different single and composite structured materials has been studied from TEM images (Fig. 3). As it can be seen, BiPO₄ presents roundish particles with sizes between

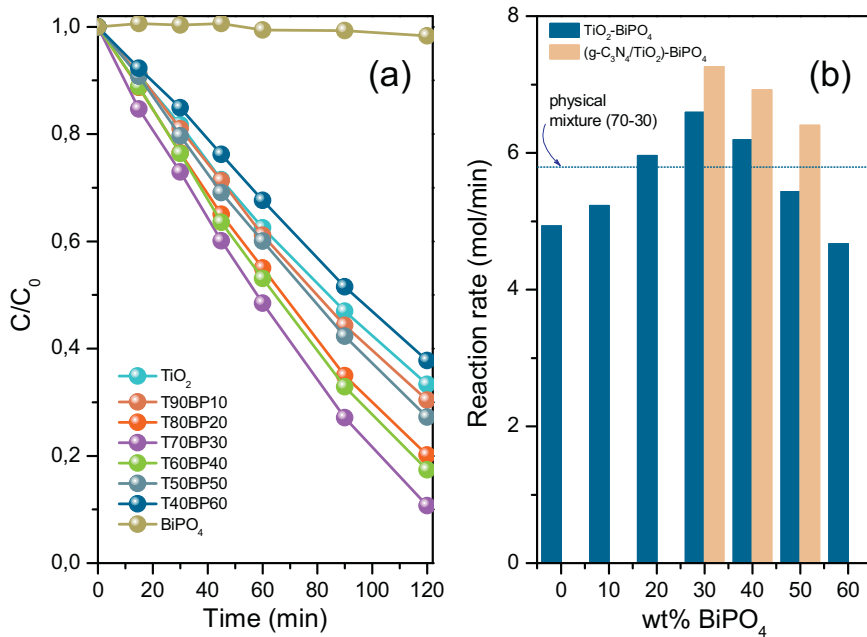


Fig. 5. (a) Phenol degradation plots; (b) reaction rates for different TiO_2 - BiPO_4 heterostructures.

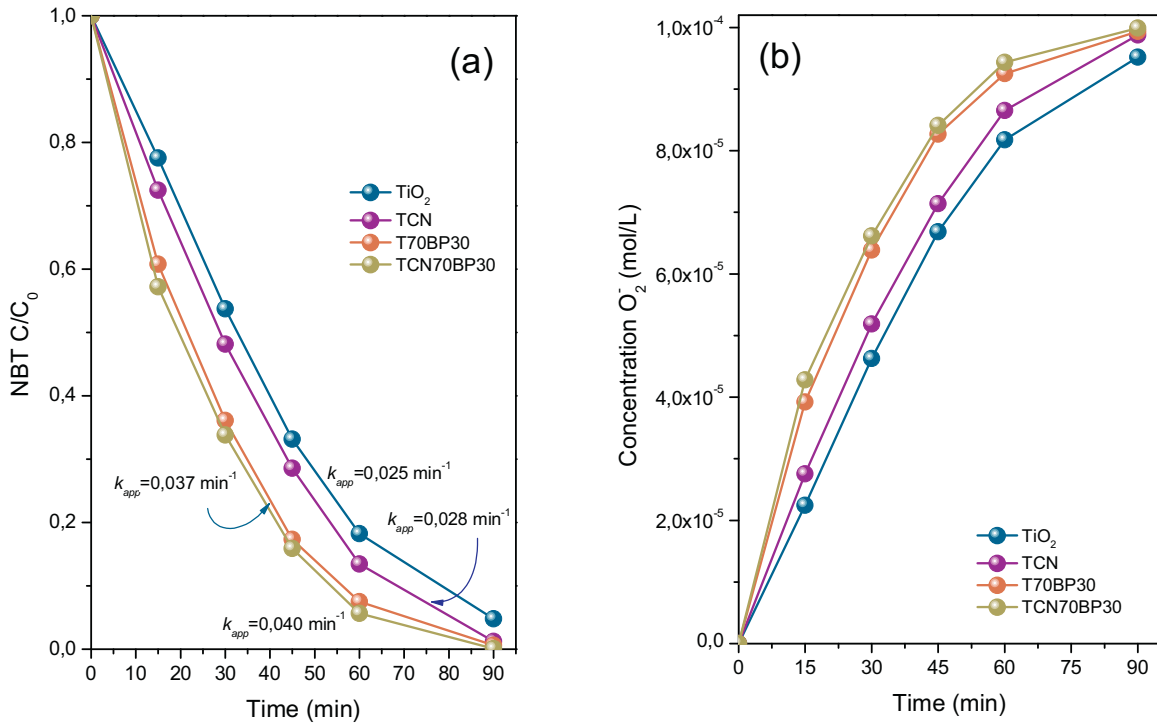


Fig. 6. (a) NBT disappearance plot; (b) superoxide formation for different TiO_2 - BiPO_4 heterostructures.

70 and 90 nm, in well accordance with the crystallite size obtained from Scherrer equation (Fig. 3a). From the selected TEM image of the heterostructured TBP system it can be stated that small TiO_2 nanoparticles seems to intimately cover the BiPO_4 particles (Fig. 3b). Similarly, TiO_2 - gC_3N_4 composite shows also the close covering of TiO_2 over large gC_3N_4 particles (Fig. 3c). Finally, the complex BiPO_4 - TiO_2 - gC_3N_4 system evidences the contact of the three components (Fig. 3d). In this later case and due to the particular preparation sequence followed, small TiO_2 particles appear as the contact point between BiPO_4 particles and gC_3N_4 .

Regarding to UV-vis absorption properties, the diffuse reflectance UV-vis spectra of different composites are shown in Fig. 4. As it can be noticed, TiO_2 and BiPO_4 semiconductors show clear different absorption edges. Thus while TiO_2 edge is placed at 390 nm, BiPO_4 would absorb photons with wavelength lower than 300 nm. Thus the calculated band gap values for those pristine semiconductors are ca. 3.2 and 4.1 eV respectively, in both cases in accordance to the reported values. In the case of BiPO_4 , it can be also noticed a small intensity long tail absorption along the visible range. Such tiny absorption could be related to the presence

of certain mid-gap states associated to structural defects [31,32]. As previously reported by us, the presence of this small absorption could be associated to the presence of oxygen vacancies probably formed during the preparation procedure upon phosphoric acid treatment [25]. On the other hand and as expected, for different composite heterojunctions the diffuse reflectance spectra show a typical profile resulting from the combination of both single spectra. In Table 1 we summarize the band gap values for TiO₂ in the TBP systems.

The photocatalytic properties of the different single, binary and ternary heterostructured systems have been followed for the phenol degradation reaction (Fig. 5). As a first remark, it is worthy to note that while TiO₂ is able to degrade more than 60% after 2 h, BiPO₄ sample exhibits a negligible photodegradation of phenol under the present experimental conditions. The assembly of TiO₂ and BiPO₄ semiconductors clearly leads to a significant improvement in the photocatalytic performance. Thus the best reaction rate is achieved for the sample with 30 wt% of BiPO₄ (T70BP30). In spite of the lower amount of TiO₂ and the significant specific surface area reduction for this composite (77 m²/g vs 115 m²/g), the calculated reaction rate is 30% higher than the corresponding for pristine TiO₂ (Table 1). Moreover, the physical mixture TiO₂-BiPO₄ with this similar 70:30 proportion shows a lower reaction rate with respect to the impregnated one. This fact would point out that the intimate junction achieved by the impregnation method, as denoted from TEM image, is playing a crucial role in the reaction mechanism. From these considerations, a clear synergistic mechanism might be proposed. The better charge separation process would be the responsible for this notably improvement as it will be discussed later.

Finally we have considered the incorporation of gC₃N₄ into the TiO₂-BiPO₄ composite in order to form a ternary heterostructure composite. As previously described, the relative band position between TiO₂ and gC₃N₄ would induce a better charge separation process [28]. Thus, the incorporation of 2 wt% of gC₃N₄ on TiO₂, forming (TiO₂-gC₃N₄)-BiPO₄ heterostructured photocatalyst (TCNBP) leads to an additional improvement as noticed from reaction rates in Fig. 5b. The observed enhancement in the reaction rate for these ternary heterojunctions is higher as BiPO₄ weight ratio is increasing. Thus, for T50BP50 sample the incorporation of gC₃N₄ induces a notably improvement effect if compared with T70BP30 sample. This would be related to the lower relative amount of gC₃N₄ with respect to BiPO₄. In this sense, we have to take into account that the loading percentage of g-C₃N₄ in the heterostructure is notably low and in addition, its intrinsic photoactivity is significantly lower than TiO₂ [28]. Therefore, upon these considerations it is reasonable to argue that the contribution to the heterostructure photoactivity could be considered practically insignificant. Thus, its contribution in the heterostructured system should be associated exclusively to the photogenerated charge separation in the electronic mechanism as will be discussed later.

It has been widely stated that the reduction of molecular oxygen is important because it is an essential part of the photocatalytic processes taking place on photocatalyst particles [33]. In some cases, the reduction of molecular oxygen determines the efficiency of the overall photocatalytic reaction, in other words, the ease of oxygen reduction on the semiconductor surface leads to a highly efficient reaction. It is generally accepted that, on TiO₂ surface, oxygen reduction reaction proceeds by a series of sequential single-electron reduction reactions and concomitantly with the formation of various reactive oxygen species such as O₂[−], HO₂[•] or H₂O₂ [34].

Thus, in order to assess the origin of the photocatalytic improvement observed in our complex heterostructured junction, we have followed the formation of superoxide radical (O₂[−]) during the irradiation of different photocatalyst. For this purpose nitroblue tetrazolium (NBT), which specifically reacts with O₂[−] and produces

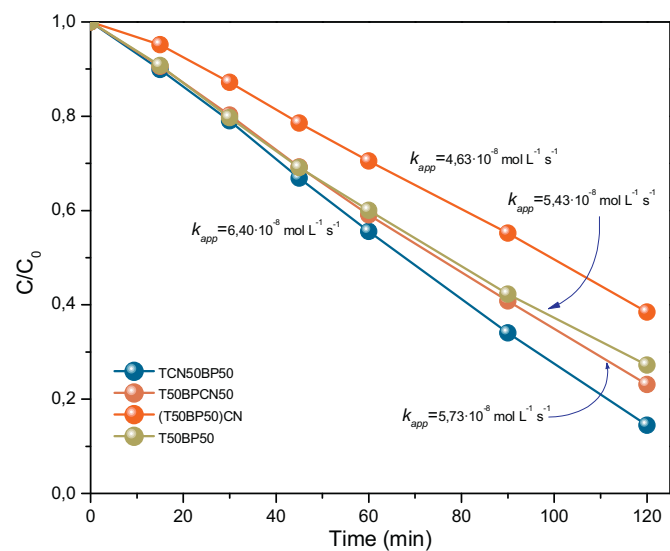


Fig. 7. Phenol degradation plots for different gC₃N₄-TiO₂-BiPO₄ (TiO₂-BiPO₄ ratio 50:50) heterostructures.

a purple precipitated [35,36], was chosen as a molecular probe to quantify the superoxide concentration and therefore the effective diffusion of photogenerated electrons in the photocatalyst.

In Fig. 6, we show the evolution of NBT disappearance and the subsequent formation of superoxide radicals. As it can be seen the TBP heterojunction clearly induces a notably increase in the formation of O₂[−] radicals. This fact could be feasibly related to the better photogenerated charge pairs separation. Similarly the formation of a complex TCNBP heterostructure prompts a slight enhancement in the formation of superoxide radicals explaining the better photoactivity observed for this system.

In the preparation section, we emphasized the fact that TiO₂ would act as contact point between BiPO₄ and gC₃N₄. Indeed, when we prepare the ternary composite by changing the impregnation sequence we obtain a noteworthy worst photoactivity (Fig. 7). If we observe the phenol degradation curves for TCN50BP50, T50BPCN50 (in this sample gC₃N₄-BiPO₄ was firstly formed) and “TBPCN” (obtained by simultaneous impregnation of TiO₂, BiPO₄ on gC₃N₄), it is clear that the most active heterojunction is that in which TiO₂ would act a contact point between BiPO₄ and gC₃N₄ (TCN50BP50). Surprisingly, “TBPCN” sample showed worst photoactivity than T50BP50, indicating a negatively effect of a random disposition. We have chosen 50-50 heterostructure since for this sample the incorporation of gC₃N₄ produces the higher improvement with respect to TBP system.

From these results it arises that the joint assembly of gC₃N₄, TiO₂ and BiPO₄ leads to a notably improvement on the photoactivity. Such better photocatalytic performance is clearly related to the particular morphological conformation of the composite which induces a better electron-hole separation. In this sense PL spectroscopy has been used in order to study the recombination processes taking place on these systems (Fig. 8a). Upon excitation with 270 nm light the emission spectra of different systems denotes that the recombination process in ternary gC₃N₄-TiO₂-BiPO₄ heterojunction is lower than TiO₂-BiPO₄ and TiO₂.

In order to explain the better photocatalytic performance of the heterostructure composite it is necessary to examine the band electronic diagram of single catalysts. Thus, the band structure of BiPO₄ could be calculated according to the following empirical equations [Eqs. (1) and (2)] [37,38]:

$$E_{VB} = \chi - E^e + 0.5 \times E_g \quad (1)$$

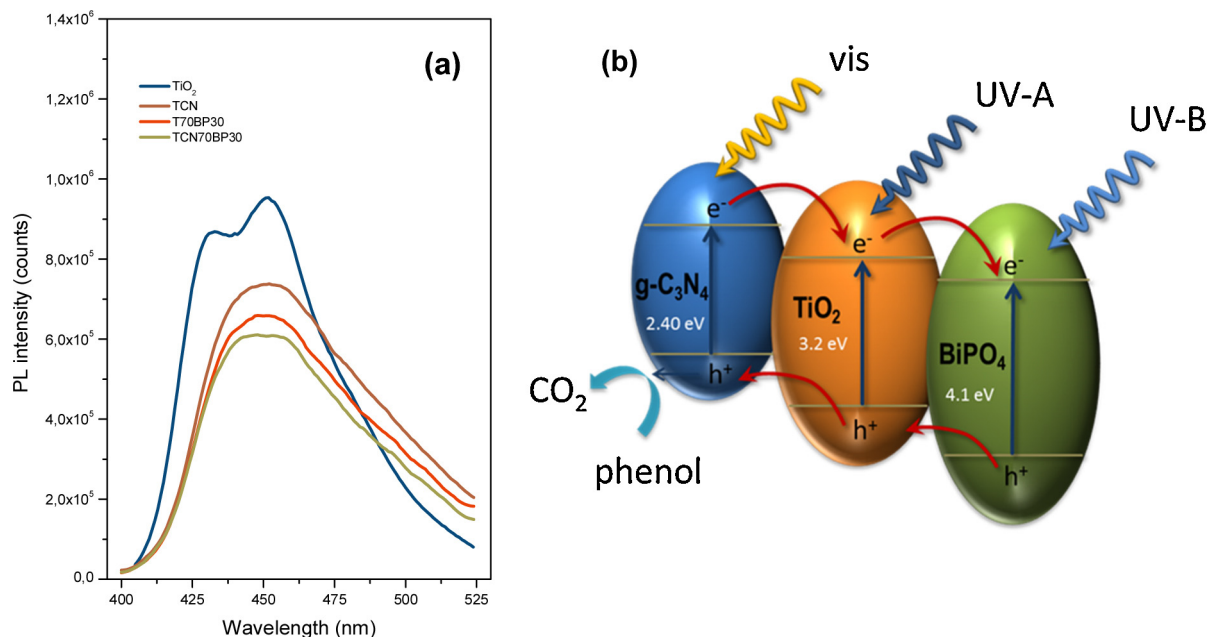


Fig. 8. (a) Photoluminescence emission spectra upon excitation at 270 nm for selected samples; (b) proposed cascade-driven electronic mechanism.

$$E_{CB} = E_{VB} - Eg \quad (2)$$

in which E_{VB} is the valence band edge potential and E_{CB} is the conduction band edge potential; χ is the electronegativity of the semiconductor, calculated as the geometric mean of the constituent atoms; and E^e is the energy of free electrons on the hydrogen scale (≈ 4.5 eV vs. NHE). From this calculation, the values for E_{VB} and E_{CB} are +0.5 and +4.6 eV, respectively. These values are in accordance with the values reported in the literature [39].

So, we can say that BiPO_4 is an n-type semiconductor for which the conduction band minimum lies rather higher than the TiO_2 ($E_{CB} = -0.5$ eV) and the top of the valence band for BiPO_4 is located at a higher position than the TiO_2 VB ($E_{VB} = +2.7$ eV) (Fig. 8b) [40]. Upon UV irradiation, both BiPO_4 and TiO_2 can be excited and produce photogenerated electron–hole pairs. Since the VB of BiPO_4 is located at higher position than the corresponding of TiO_2 , the photogenerated holes on BiPO_4 can directly transfer to TiO_2 , making charge separation more efficient and reducing the probability of photogenerated electron–hole recombination, resulting in an enhanced photocatalytic activity.

Thus, such particular junction in which TiO_2 would act as contact point would lead to the best electron–hole separation scheme (Fig. 8b). The proposed system would be excited by different energy photons (UV-A, UV-B and visible in lower extent). Then an effective cascade driven separation mechanism would induce the significantly higher photocatalytic performance.

4. Conclusions

By a simple impregnation method and taking into consideration the relative band positions, we have obtained a complex $\text{g-C}_3\text{N}_4$ – TiO_2 – BiPO_4 heterostructured system exhibiting a notably improved photoactivity with respect to the single semiconductors. Thus the optimum phenol degradation rate for such assembled photocatalyst is 1.5 times higher with respect to pristine TiO_2 . Considering that TiO_2 participation in this heterostructure is 70 wt% it can be said that this is a significant enhancement. Photoluminescence analysis as well as superoxide formation study clearly denotes a better charge separation mechanism. A cascade-driven electronic mechanism is proposed to explain the photoactivity enhancement.

Therefore, by means band engineering tailoring and the adequate junction of selected semiconductors it is possible to progressively increase the photocatalytic efficiency of the process.

Acknowledgments

S. Obregón also thanks CSIC for the concession of a JAE-Pre grant. The financial support by projects P09-FQM-4570 and ENE2011-24412 is fully acknowledged.

References

- [1] G. Colón, C. Belver, M. Fernández-García, Nanostructured oxides in photocatalysis, in: J.A. Rodríguez, M. Fernández-García (Eds.), *Synthesis, Properties and Applications of Solid Oxides*, Wiley, New York, 2007.
- [2] A. Kubacka, M. Fernández-García, G. Colón, *Chem. Rev.* 112 (2012) 1555–1614.
- [3] M. Hoffmann, S. Martin, W. Choi, D. Bahnemann, *Chem. Rev.* 95 (1995) 69–96.
- [4] M.A. Henderson, *Surf. Sci. Rep.* 66 (2011) 185–297.
- [5] F. Lin, D.M. Jiang, X.M. Ma, *J. Alloys Compd.* 470 (2009) 375–378.
- [6] K. Bhattacharyya, S. Varma, A.K. Tripathi, S.R. Bharadwaj, A.K. Tyagi, *J. Phys. Chem. C* 112 (2008) 19102–19112.
- [7] S. Ould-Chikh, O. Proux, P. Afanasiev, L. Khrouz, M.N. Hedhili, D.H. Anjum, M. Harb, C. Geantet, J.M. Basset, E. Puzenat, *ChemSusChem* 7 (2014) 1361–1371.
- [8] S.Z. Chen, P.Y. Zhang, D.M. Zhuang, W.P. Zhu, *Catal. Commun.* 5 (2004) 677–680.
- [9] F. Dong, W.R. Zhao, Z.B. Wu, *Nanotechnology* 19 (2008) 365607.
- [10] M. Harb, P. Sautet, P. Raybaud, *J. Phys. Chem. C* 117 (2013) 8892–8902.
- [11] M.C. Hidalgo, M. Maicu, J.A. Navío, G. Colón, *J. Phys. Chem. C* 113 (2009) 12840–12847.
- [12] G. Colón, M. Maicu, M.C. Hidalgo, J.A. Navío, A. Kubacka, M. Fernández-García, *J. Mol. Catal. A Chem.* 320 (2010) 14–18.
- [13] N. Zhang, Y. Zhang, Y.J. Xu, *Nanoscale* 4 (2012) 5792–5813.
- [14] P. Niu, L. Zhang, L. Liu, H.M. Cheng, *Adv. Funct. Mater.* 22 (2012) 4763–4770.
- [15] S. Zhao, S. Chen, H. Yu, X. Quan Sep, *Purif. Technol.* 99 (2012) 50–54.
- [16] S.K. Poznyak, D. Talapin, A. Kulak, J. Phys. Chem. B 105 (2001) 4816–4823.
- [17] Y. Peng, M. Yan, Q.G. Chen, C.M. Fan, H.Y. Zhou, A.W. Xu, *J. Mater. Chem. A* 2 (2014) 8517–8524.
- [18] S. Bera, S.B. Rawal, H.J. Kim, W.I. Lee, *ACS Appl. Mater. Interfaces* 6 (2014) 9654–9663.
- [19] R. Marschall, *Adv. Funct. Mater.* 24 (2014) 2421–2440.
- [20] Y. Peng, Q.G. Chen, D. Wang, H.Y. Zhou, A.W. Xu, *CrystEngComm* 17 (2015) 569–576.
- [21] M. Wang, D. Zheng, M. Ye, C. Zhang, B. Xu, C. Lin, L. Sun, Z. Lin, *Small* 11 (2015) 1436–1442.
- [22] B. Gao, Y.J. Kim, A.K. Chakraborty, W.I. Lee, *Appl. Catal. B Environ.* 83 (2008) 202–207.
- [23] S. Bera, S.B. Rawal, H.J. Kim, W.I. Lee, *ACS Appl. Mater. Interfaces* 6 (2014) 9654–9663.

- [24] M. Woodhouse, B.A. Parkinson, *Chem. Soc. Rev.* 38 (2009) 197–210.
- [25] Y. Zhang, M. Sillanpää, S. Obregón, G. Colón, *J. Mol. Catal. A* 402 (2015) 92–99.
- [26] M.C. Hidalgo, M. Aguilar, M. Maicu, J.A. Navío, G. Colón, *Catal. Today* 129 (2007) 50–58.
- [27] S.C. Yan, Z.S. Li, Z.G. Zou, *Langmuir* 25 (2009) 10397–10401.
- [28] C. Miranda, H. Mansilla, J. Yáñez, S. Obregón, G. Colón, *J. Photochem. Photobiol. A Chem.* 253 (2013) 16–21.
- [29] C. Pan, J. Xu, Y. Wang, D. Li, Y. Zhu, *Adv. Funct. Mater.* 22 (2012) 1518–1524.
- [30] H. Goto, Y. Hanada, T. Ohno, M. Matsumura, *J. Catal.* 225 (2004) 223–229.
- [31] C. Pan, Y. Zhu, *J. Mater. Chem.* 21 (2011) 4235–4241.
- [32] Y. Lv, Y. Liu, Y. Zhu, Y. Zhu, *J. Mater. Chem. A* 2 (2014) 1174–1182.
- [33] S.A.J. Moniz, S.A. Shevlin, X. An, Z.X. Guo, J. Tang, *Chem. Eur. J.* 20 (2014) 15571–15579.
- [34] H. Sheng, H. Ji, W. Ma, C. Chen, J. Zhao, *Angew. Chem. Int. Ed.* 52 (2013) 9686–9690.
- [35] L. Ye, J. Liu, C. Gong, L. Tian, L. Peng, L. Zan, *ACS Catal.* 2 (2012) 1677–1683.
- [36] L. Ye, J. Liu, Z. Jiang, T. Peng, L. Zan, *Nanoscale* 5 (2013) 9391–9396.
- [37] S. Obregón, G. Colón, *Appl. Catal. B Environ.* 140–141 (2013) 299–305.
- [38] H. Huang, S. Wang, Y. Zhang, P.C. Chu, *RSC Adv.* 4 (2014) 41219–41227.
- [39] F. Duo, Y. Wang, X. Mao, X. Zhang, Y. Wang, C. Fan, *Appl. Surf. Sci.* 340 (2015) 35–42.
- [40] H. Xu, Y. Xu, H. Li, J. Xia, J. Xiong, S. Yin, C. Huang, H. Wan, *Dalton Trans.* 41 (2012) 3387–3394.